CrystEngComm

COMMUNICATION

View Article Online
View Journal | View Issue

Cite this: *CrystEngComm*, 2018, **20**, 4541

Received 25th April 2018,
Accepted 22nd June 2018

DOI: 10.1039/c8ce00662h

rsc.li/crystengcomm

Trisiloxane-centred metal–organic frameworks and hydrogen bonded assemblies†

Luke C. Delmas, [a] Andrew J. P. White,[a] David Pugh, [a] Peter N. Horton,[b] Simon J. Coles, [b] Paul D. Lickiss *[a] and Robert P. Davies *[a]

A hexacarboxylic acid with a trisiloxane backbone (**L**-H_6) has been prepared and applied in MOF construction. **L**-H_6 itself crystallizes as an unusual 2D hydrogen-bonded network. Reaction of **L**-H_6 with Mn(II) gave **IMP-20** and with Zn(II) gave **IMP-21**: both are 3D MOFs incorporating Si–O–Si–O–Si linkages.

The notable potential of metal–organic frameworks (MOFs) to act as functional materials for a wide range of applications,[1] coupled with their controllable and modular synthesis[2] has led to a proliferation of studies on these materials.[3] The application of highly connected linkers for MOF construction is an area of particular interest since these linkers have been shown to enable the preparation of MOFs with new topologies[4,5] often with enhanced framework stability.[6] Research in our group has focussed upon the use of highly branched organosilicon linkers, which are notable for their convenient synthesis, and their use in the construction of 3D MOFs.[7–9] More recently we have shown how linkers with disiloxane backbones, such as hexakis(4-carboxyphenyl)disiloxane ($R_3Si–O–SiR_3$, R = *p*-C_6H_4COOH), can be used to prepare novel porous 3D coordination polymers that may loosely be described as hybrid MOF-zeolite systems (the siloxane Si–O–Si linkage being ubiquitous in zeolites).[10] Installing siloxane linkages in MOFs may impart several advantageous properties including low chemical reactivity, high thermal stability, hydrophobicity, and enhanced water stability.[10–12] In an extension to this earlier work, we now report upon the preparation and application of a hexacarboxylic acid with a trisiloxane backbone, $R_3Si–O–SiMe_2–O–SiR_3$ (R = *p*-C_6H_4COOH), **L**-H_6. Extension of the siloxane moiety to incorporate a central tetrahedral dimethylsilyl functionality leads to a U-shaped Si–O–Si–O–Si backbone in **L**-H_6 which contrasts with the approximately linear Si–O–Si backbone in the previously reported disiloxane.[10] The resultant change in the disposition of the six benzoic acid groups on the linker backbone is reflected in the unique structural forms observed in the hydrogen-bonded assembly of **L**-H_6 and its coordination complexes.

The synthesis of the novel connector **L**-H_6 is outlined in Scheme 1. Firstly, tris(4-bromophenyl)silanol[13] was treated with pyridine and then allowed to react with dimethyldichlorosilane to produce the corresponding trisiloxane. Treatment with six molar equivalents of *n*-BuLi, followed by reaction of the polylithiated intermediate with CO_2 and acidic workup affords **L**-H_6.

A number of highly branched polycarboxylic acids have been reported to assemble into extended supramolecular structures through dimeric hydrogen bonding of their acid groups, leading to materials with interesting properties such as permanent porosity and selective gas adsorption.[10,14–21]

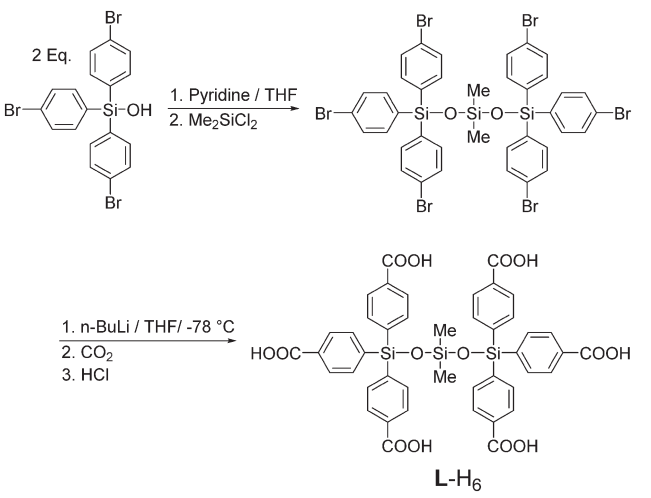

Scheme 1 Synthesis of **L**-H_6.

[a] *Department of Chemistry, Imperial College London, South Kensington, London, SW7 2AZ, UK. E-mail: p.lickiss@imperial.ac.uk, r.davies@imperial.ac.uk*
[b] *EPSRC Crystallographic Service, Department of Chemistry, University of Southampton, Highfield, Southampton, SO17 1BJ, UK*

† Electronic supplementary information (ESI) available: Full experimental details of the synthesis, characterisation data, crystallographic protocols, PXRD and TGA plots for **IMP-20** and **IMP-21**. CCDC 1836630–1836632. Details of topological analyses for structures are also presented. For ESI and crystallographic data in CIF or other electronic format see DOI: 10.1039/c8ce00662h

Given the unusual arrangement of the six carboxylic acid groups in **L**-H_6, we were interested in determining its H-bonded superstructure. Single crystals of **L**-H_6 can be obtained by slow evaporation from a mixture of AcOH and MeOH. X-ray analysis reveals that **L**-H_6 crystallizes as the **L**-H_6·AcOH·$\frac{1}{2}H_2O$ solvate in the monoclinic space group $P2/n$ (no. 13) and the asymmetric unit contains two crystallographically distinct molecules of **L**-H_6, two molecules of acetic acid and a molecule of water. The tetrahedral geometry of the central Si unit in **L** results in a U-shaped trisiloxane backbone. The angles formed between the three silicon atoms in the backbone are 101.92(5)° and 100.16(5)° (for the two crystallographically independent **L** molecules) and the Si–O–Si bond angles lie in the range 139.8(2)–156.1(2)° (mean 150.2°).

All carboxylic acid groups of **L**-H_6 participate in hydrogen-bonding interactions either with neighbouring **L**-H_6 molecules or acetic acid to afford a remarkably complicated polymeric structure (*vide infra*). The dimeric H-bonding O···O distances are all in the range 2.579(7)–2.750(5) Å, typical of strong hydrogen bonds,[22–24] and the unusual parallel arrangement of two of the acid groups on each **L**-H_6 molecule results in a set of rare 'quadruple H-bonds' between some of the molecules as shown in Fig. 1a.

The **L**-H_6 molecules can be considered to form a polymeric structure *via* hydrogen bonding to give 1-dimensional coiled strands along the crystallographic *a* direction. These strands are triply intertwined resulting in a triply-braided molecular bundle (Fig. 1b). Such multistranded helical assembles built from achiral small molecules are particularly rare.[25] The triply-braided bundles are further interlinked *via* their peripheral COOH groups to neighbouring bundles to give 2D corrugated layers (Fig. 1c). These layers are prevented from aggregating to a 3D network by the presence of AcOH groups which 'cap' the remaining pendant carboxylates.

We then turned our attention to the complexation of **L**-H_6 with transition metal cations for the generation of new metal–organic framework materials. The reaction of **L**-H_6 with $Mn(OAc)_2$·$4H_2O$ in a 10 : 1 mixture of DMF/AcOH at 120 °C for 2 days afforded colourless needles. These crystals were characterised by single crystal X-ray analysis to be $[Mn_3(\mathbf{L})(DMF)_4]$·6DMF (**IMP-20**, where IMP is short for Imperial College London) and the bulk purity of the sample was confirmed by powder X-ray diffraction (Fig. S4†).[26] The crystals were found to comprise a 3D MOF built from discrete trimetallic nodes linked together by the fully deprotonated hexa-anionic **L** linker (Fig. 2). The angle formed between the three silicon atoms in the ligand backbone is 100.24(6)° and the Si–O–Si bond angles are both bent at 140.22(18)°. Although the linker has 6 coordinating groups, a single molecule of **L** only binds to 4 metal nodes. This is because there are two parallel pairs of carboxyphenyl rings within each **L**, each of which coordinates to a single metal node or SBU (secondary building unit), see Fig. 2a. This type of coordination behaviour has been previously reported in MOFs built from flexible linkers.[27] The inorganic nodes comprise a known arrangement[28,29] of three Mn atoms held together by six bridging dimonodentate carboxylates (from 4 different ligands) with the coordination sphere of the outer Mn(II) ions completed by coordinating solvent molecules. This therefore leads to a (4,4)-connected net of **PtS** topology, assuming each **L** unit is considered as 4-connected. An alternative topology for **IMP-20** can be described when considering the terminal silicon atoms as two linked 4-connected vertices. This results in an unreported (4,6)-connected 3-dimensional net whose point symbol is $\{3^2{\cdot}4^2{\cdot}5{\cdot}6\}_2\{3^2{\cdot}4^2{\cdot}5^2{\cdot}8^7{\cdot}9{\cdot}10\}$ – see Fig. S7.† The **IMP-20** framework has solvent-filled channels with the largest window size being approximately 10 × 7 $Å^2$ (atom to atom distance) along the [101] direction. After theoretical removal of the non-coordinated solvent, the PLATON[30] predicted solvent-accessible void volume for **IMP-20** was found to be 4226.9 $Å^3$ or 45% of the unit cell volume.

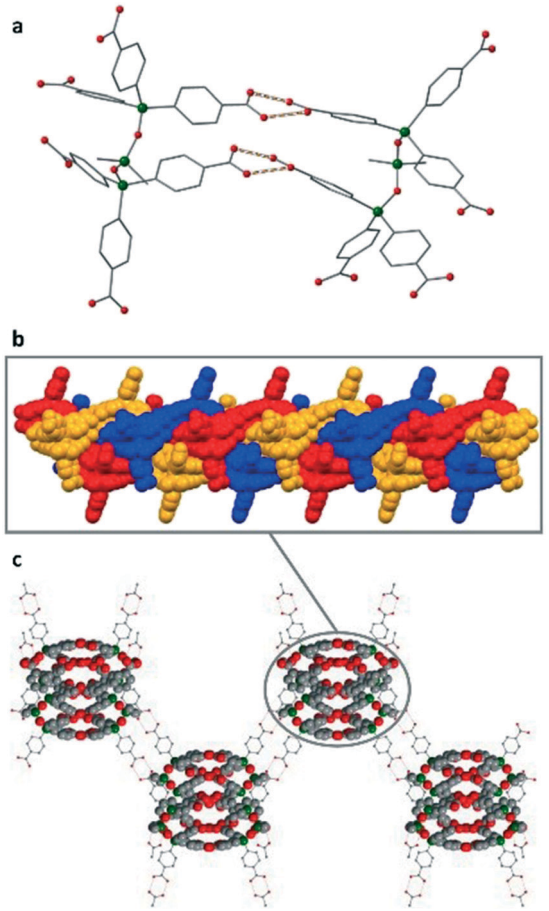

Fig. 1 (a) Quadruple H-bonding between two neighbouring molecules of **L**-H_6, (b) space-filling model of three coils of molecules mutually intertwined to afford a tightly-knit molecular bundle, (c) four separate molecular bundles linked *via* H-bonding of their pendant COOH groups to form a corrugated layer (view along *a* axis). Colour scheme for molecular structures: O shown in red; C, grey; Si, green. Hydrogen atoms are not shown for clarity.

Reaction of **L**-H_6 with anhydrous $Zn(OAc)_2$ in a 10 : 1 mixture of DMF/AcOH at 120 °C in a sealed vessel for 2 days afforded colourless needle-like crystals of **IMP-21** (Fig. 3). These crystals were characterised by single crystal X-ray

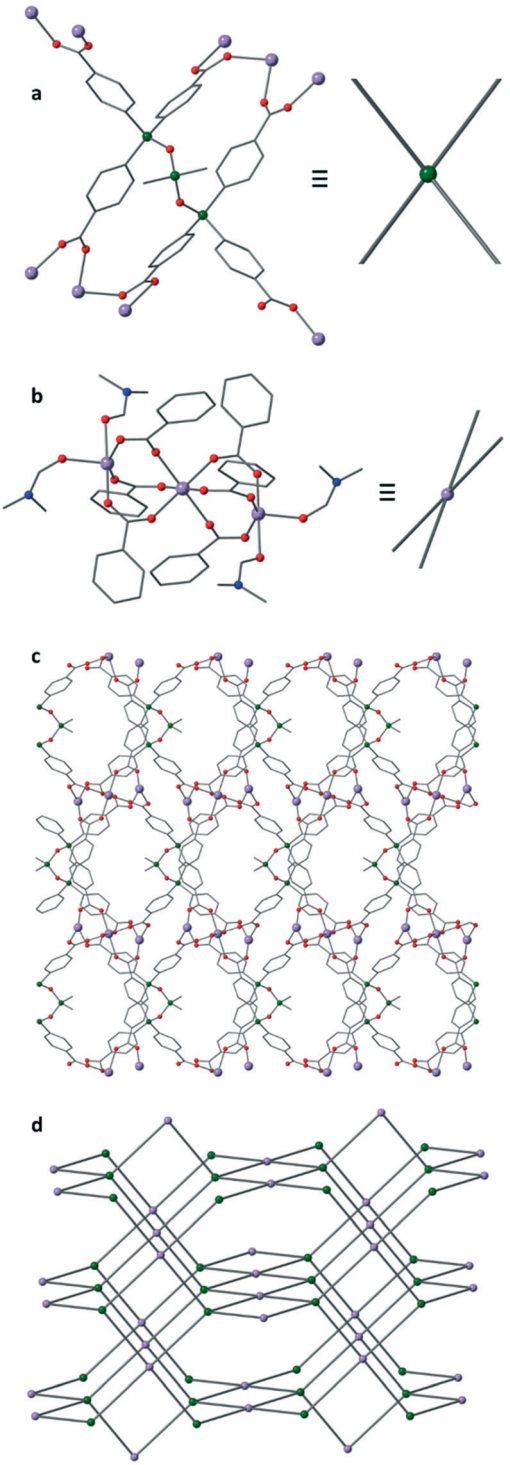

Fig. 2 (a) Ligand environment of **L** in **IMP-20**. (b) Structure of trinuclear manganese SBUs in **IMP-20**. (c) Portion of the extended structure of **IMP-20** showing channels along the crystallographic *a* direction. Disorder, solvent molecules, and hydrogen atoms omitted for clarity. Colour scheme: Mn, purple; O, red; C, grey; Si, green; N, dark blue. (d) Schematic representation of the **PtS** network showing the 4-connected Mn SBU nodes (purple) and the 4-connected silicon-based nodes (green).

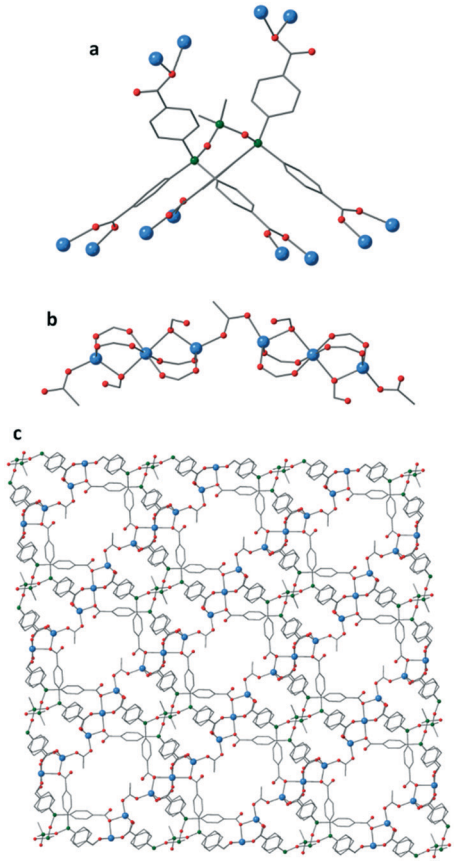

Fig. 3 (a) Coordination environment of **L** in **IMP-21**. (b) Portion of Zn-based rod SBU in **IMP-21** showing acetate group bridging trimetallic clusters. (c) Section of **IMP-21** viewed along the crystallographic *b* axis – disorder, solvent molecules and hydrogen atoms omitted for clarity. Colour scheme: Zn, blue; O, red; C, grey; Si, green.

analysis to be $[Zn_3(\mathbf{L})(OAc)][Me_2NH_2]\cdot 3.75DMF$ and the bulk purity of the sample was confirmed by powder X-ray diffraction (Fig. S8†). The crystals were found to comprise a porous 3D-connected MOF built from zinc-based rod[31] secondary building units (SBUs) linked together by the fully deprotonated ligand **L**.

IMP-21 is an anionic framework with the asymmetric unit containing one molecule of **L** and one acetate to just three Zn(II) cations. The overall negative charge is most likely balanced by the presence of disordered dimethylammonium cations in the pores of the MOF. Evidence for this was obtained using ^{1}H NMR studies of the digested MOF in aqueous NaOD which showed a signal at 1.75 ppm attributable to dimethylamine (see ESI† for further information). These balancing dimethylammonium cations can be formed by decomposition of DMF solvent molecules under solvothermal conditions, and have been previously reported for a number of other MOFs.[7,32] The angle formed between the three silicon atoms in the backbone of **L** is 119.67(4)°, significantly more obtuse than in the structures of **L**-H_6 and **IMP-20** (see Fig. S12† for comparison). This gives rise to a widened U-shaped conformation of the ligand. The trisiloxane group in **IMP-21** has one siloxane linkage which is significantly

more bent than the other [<Si–O–Si 143.08(13)° and 159.65(14)°], highlighting the flexibility of the trisiloxane unit. Overall, **L** can be viewed as a 3-connected node in this MOF since there are three pairs of parallel acid groups which each bind to a separate zinc-based rod SBU.[31] The metal secondary building units are constructed of trimetallic zinc clusters linked together by bridging dimonodentate acetate units to afford 1D polymeric SBUs which run in the [101] direction. An alternative approach in which the bridging acetate group is considered as a linear 2-c node, leads to an interpretation where the trimetallic metal clusters can be viewed as 8-c vertices connected by the ligand **L** (viewed as two conjoined 4-c vertices) thus giving rise to a new (4,8)-connected topology whose point symbol is $\{4^{12}\cdot6^{12}\cdot8^{4}\}\{4^{6}\}_2$ – see Fig. S11† for further analysis. The **IMP-21** structure contains solvent-filled channels in all three dimensions with the largest channels lying along the [101] direction with measurements of approximately 8 × 7 Å^2, followed by those in the direction of the crystallographic *b* axis whose dimensions are approximately 9 × 6 Å^2. After theoretical removal of the non-coordinated solvent and charge-balancing cations, PLATON[30] predicts a solvent-accessible void volume for **IMP-21** of 5611.6 Å^3 or 41% of the unit cell volume.

Despite the potential void space reported for **IMP-20** and **21**, both materials underwent decomposition during activation and therefore were unsuitable for further porosity studies.

In summary, the novel hexacarboxylic acid linker with trisiloxane backbone **L**-H_6 has been prepared and shown to self-assemble into a unique hydrogen-bonded network based on triply-braided strands. Treatment of **L**-H_6 with Mn(II) and Zn(II) salts gave **IMP-20** and **IMP-21**, respectively, which to the best of our knowledge are the first 3D-connected MOF structures incorporating a trisiloxane linker. The trisiloxane unit displays some flexibility allowing **L** to adjust its backbone geometry, thus extending or contracting its reach in order to optimise binding to metal nodes in MOFs. This flexibility may lend itself to the design of other dynamic MOFs which show breathing behaviour.[33,34] We are also interested in preparing other trisiloxane-based systems noting that the central silicon atom is an obvious choice for further functionalization (*e.g.* with OH groups) that could lead to porous MOFs with unique properties.

The Imperial College President's Scholarship Scheme (L. D.) and the EPSRC (EP/M507878/1) are acknowledged for funding this work. We are grateful to W. T. Klooster at the EPSRC UK National Crystallography Service at the University of Southampton for the collection of the crystallographic data for **IMP-21**.

Conflicts of interest

There are no conflicts to declare.

Notes and references

1 C. Pettinari, F. Marchetti, N. Mosca, G. Tosi and A. Drozdov, *Polym. Int.*, 2017, **66**, 731–744.
2 H. Furukawa, K. E. Cordova, M. O'Keeffe and O. M. Yaghi, *Science*, 2013, **341**, 1230444.
3 P. Z. Moghadam, A. Li, S. B. Wiggin, A. Tao, A. G. P. Maloney, P. A. Wood, S. C. Ward and D. Fairen-Jimenez, *Chem. Mater.*, 2017, **29**, 2618–2625.
4 W. Lu, Z. Wei, Z.-Y. Gu, T.-F. Liu, J. Park, J. Park, J. Tian, M. Zhang, Q. Zhang, T. Gentle III, M. Bosch and H.-C. Zhou, *Chem. Soc. Rev.*, 2014, **43**, 5561–5593.
5 F. A. Almeida Paz, J. Klinowski, S. M. F. Vilela, J. P. C. Tome, J. A. S. Cavaleiro and J. Rocha, *Chem. Soc. Rev.*, 2012, **41**, 1088–1110.
6 S. Yuan, L. Feng, K. Wang, J. Pang, M. Bosch, C. Lollar, Y. Sun, J. Qin, X. Yang, P. Zhang, Q. Wang, L. Zou, Y. Zhang, L. Zhang, Y. Fang, J. Li and H.-C. Zhou, *Adv. Mater.*, 2018, DOI: 10.1002/adma.201704303.
7 R. P. Davies, R. Less, P. D. Lickiss, K. Robertson and A. J. P. White, *Cryst. Growth Des.*, 2010, **10**, 4571–4581.
8 R. P. Davies, P. D. Lickiss, K. Robertson and A. J. P. White, *CrystEngComm*, 2012, **14**, 758–760.
9 I. Timokhin, A. J. P. White, P. D. Lickiss, C. Pettinari and R. P. Davies, *CrystEngComm*, 2014, **16**, 8094–8097.
10 L. C. Delmas, P. N. Horton, A. J. P. White, S. J. Coles, P. D. Lickiss and R. P. Davies, *Chem. Commun.*, 2017, **53**, 12524–12527.
11 C. Racles, M.-F. Zaltariov, M. Iacob, M. Silion, M. Avadanei and A. Bargan, *Appl. Catal., B*, 2017, **205**, 78–92.
12 B. Sels and L. Kustov, *Zeolites and Zeolite-like Materials*, Elsevier, Amsterdam, 2016.
13 H. Ma, D. Sun, L. Zhang, R. Wang, V. A. Blatov, J. Guo and D. Sun, *Inorg. Chem.*, 2013, **52**, 10732–10734.
14 I. Hisaki, S. Nakagawa, N. Tohnai and M. Miyata, *Angew. Chem., Int. Ed.*, 2015, **54**, 3008–3012.
15 C. A. Zentner, H. W. H. Lai, J. T. Greenfield, R. A. Wiscons, M. Zeller, C. F. Campana, O. Talu, S. A. FitzGerald and J. L. C. Rowsell, *Chem. Commun.*, 2015, **51**, 11642–11645.
16 S. Nandi, D. Chakraborty and R. Vaidhyanathan, *Chem. Commun.*, 2016, **52**, 7249–7252.
17 I. Hisaki, N. Ikenaka, N. Tohnai and M. Miyata, *Chem. Commun.*, 2016, **52**, 300–303.
18 I. Hisaki, S. Nakagawa, N. Ikenaka, Y. Imamura, M. Katouda, M. Tashiro, H. Tsuchida, T. Ogoshi, H. Sato, N. Tohnai and M. Miyata, *J. Am. Chem. Soc.*, 2016, **138**, 6617–6628.
19 J. L. Segura, R. Juarez, M. Ramos and C. Seoane, *Chem. Soc. Rev.*, 2015, **44**, 6850–6885.
20 I. Hisaki, N. Ikenaka, E. Gomez, B. Cohen, N. Tohnai and A. Douhal, *Chem. – Eur. J.*, 2017, **23**, 11611–11619.
21 F. Hu, C. Liu, M. Wu, J. Pang, F. Jiang, D. Yuan and M. Hong, *Angew. Chem., Int. Ed.*, 2017, **56**, 2101–2104.
22 D. J. Duchamp and R. E. Marsh, *Acta Crystallogr., Sect. B: Struct. Sci.*, 1969, **25**, 5–19.
23 M. Bailey and C. J. Brown, *Acta Crystallogr.*, 1967, **22**, 387–391.

24 R. Alcala and S. Martinez-Carrera, *Acta Crystallogr., Sect. B: Struct. Sci.*, 1972, **28**, 1671–1677.
25 E. Yashima, N. Ousaka, D. Taura, K. Shimomura, T. Ikai and K. Maeda, *Chem. Rev.*, 2016, **116**, 13752–13990.
26 S. J. Coles and P. A. Gale, *Chem. Sci.*, 2012, **3**, 683–689.
27 C. L. Jones, E. A. Marsden, A. C. Nevin, B. M. Kariuki, M. M. Bhadbhade, A. D. Martin and T. L. Easun, *R. Soc. Open Sci.*, 2017, **4**, 171064.
28 A. Kornowicz, S. Komorski, Z. Wrobel, I. Justyniak, N. Nedelko, A. Slawska-Waniewska, R. Balawender and J. Lewinski, *Dalton Trans.*, 2014, **43**, 3048–3051.
29 C. J. Milios, T. C. Stamatatos, P. Kyritsis, A. Terzis, C. P. Raptopoulou, R. Vicente, A. Escuer and S. P. Perlepes, *Eur. J. Inorg. Chem.*, 2004, **14**, 2885–2901.
30 A. L. Spek, *J. Appl. Crystallogr.*, 2003, **36**, 7–13.
31 A. Schoedel, M. Li, D. Li, M. O'Keeffe and O. M. Yaghi, *Chem. Rev.*, 2016, **116**, 12466–12535.
32 X.-R. Hao, X.-L. Wang, Z.-M. Su, K.-Z. Shao, Y.-H. Zhao, Y.-Q. Lan and Y.-M. Fu, *Dalton Trans.*, 2009, 8562–8566.
33 R. E. Morris and L. Brammer, *Chem. Soc. Rev.*, 2017, **46**, 5444–5462.
34 G. Ferey and C. Serre, *Chem. Soc. Rev.*, 2009, **38**, 1380–1399.